energies

MDPI

Article

Experimental Research and Improved Neural Network Optimization Based on the Ocean Thermal Energy Conversion Experimental Platform

Yanni Yu [1], Mingqian Tian [1], Yanjun Liu [1,2,*], Beichen Lu [1] and Yun Chen [1,*]

1 Institute of Marine Science and Technology, Shandong University, Qingdao 266237, China; 202216957@mail.sdu.edu.cn (Y.Y.); 202221078@mail.sdu.edu.cn (M.T.); 202136988@mail.sdu.edu.cn (B.L.)
2 Key Laboratory of High-Efficiency and Clean Mechanical Manufacture of Ministry of Education, Shandong University, Jinan 250061, China
* Correspondence: lyj111@sdu.edu.cn (Y.L.); chenyuneast@mail.sdu.edu.cn (Y.C.); Tel.: +86-133-2513-6508 (Y.L.); +86-181-5322-1855 (Y.C.)

Abstract: With the progress of research on ocean thermal energy conversion, the stabI have checked and revised all. le operation of ocean thermal energy conversion experiments has become a problem that cannot be ignored. The control foundation for stable operation is the accurate prediction of operational performance. In order to achieve accurate prediction and optimization of the performance of the ocean thermal energy conversion experimental platform, this article analyzes the experimental parameters of the turbine based on the basic experimental data obtained from the 50 kW OTEC experimental platform. Through the selection and training of experimental data, a GA-BP-OTE (GBO) model that can automatically select the number of hidden layer nodes was established using seven input parameters. Bayesian optimization was used to complete the optimization of hyperparameters, greatly reducing the training time of the surrogate model. Analyzing the prediction results of the GBO model, it is concluded that the GBO model has better prediction accuracy and has a very low prediction error in the prediction of small temperature changes in ocean thermal energy, proving the progressiveness of the model proposed in this article. The dual-objective optimization problem of turbine grid-connected power and isentropic efficiency is solved. The results show that the change in isentropic efficiency of the permeable device is affected by the combined influence of the seven parameters selected in this study, with the mass flow rate of the working fluid having the greatest impact. The *MAPE* of the GBO model turbine grid-connected power is 0.24547%, the *MAPE* of the turbine isentropic efficiency is 0.04%, and the *MAPE* of the turbine speed is 0.33%. The Pareto-optimal solution for the turbine grid-connected power is 40.1792 kW, with an isentropic efficiency of 0.837439.

Keywords: GA-BP-OTEC model; ocean thermal energy conversion (OTEC); OTEC experimental platform; pareto-optimal solution

check for updates

Citation: Yu, Y.; Tian, M.; Liu, Y.; Lu, B.; Chen, Y. Experimental Research and Improved Neural Network Optimization Based on the Ocean Thermal Energy Conversion Experimental Platform. *Energies* **2024**, *17*, 4310. https://doi.org/10.3390/en17174310

Academic Editor: Efstathios E. Michaelides

Received: 2 August 2024
Revised: 20 August 2024
Accepted: 27 August 2024
Published: 28 August 2024

1. Introduction

Ocean thermal energy refers to the heat contained between warm surface seawater and deep cold seawater. As a renewable energy source, it has the advantages of being clean, pollution-free, having large reserves, and good stability [1], and is considered a highly potential and valuable marine resource for development. The essence of ocean thermal energy conversion (OTEC) is to convert thermal energy into electrical energy, which can also provide energy for large deep-sea equipment and small underwater mobile equipment [2]. The organic Rankine cycle [3], as the most basic OTEC closed cycle, has been widely studied.

In order to improve the thermal efficiency of ocean thermal energy conversion systems from a theoretical analysis perspective, extensive research has been conducted. Jung In Yoon et al. [4] proposed an efficient R717 regenerative OTEC cycle with an expansion valve and cooler, which reduces the waste heat absorbed by the condenser through the cooler and gas-liquid separator and reduces the absorbed heat through the regenerator. Miljkovic introduced an ejector into the basic Rankine cycle [5] and designed a new cycle that allows a portion of the working fluid at the condenser outlet to enter the injector, reducing the pressure at the turbine outlet. The efficiency of this cycle is 3.057%. Based on the Rankine cycle, Kalina proposed a new power cycle using an ammonia/water mixture as the working fluid—the Kalina cycle [6]. The efficiency of the Kalina cycle is 1.6–1.9 times that of the Rankine cycle. Professor Haruna Uehara of Saga University in Japan proposed a new type of closed ocean thermal energy conversion power generation cycle system, the Uehara Cycle [7], which greatly improves efficiency through the combination of two-stage turbines with intermediate extraction and the main cycle and evaporation separation cycle [8]. In 2012, the First Institute of Oceanography of the State Oceanic Administration (now the First Institute of Oceanography, MNR) proposed a new cycle method, abbreviated as the Guohai cycle. Currently, the thermal efficiency of the Guohai cycle is the highest, about 5.1% [9]. Ge Yunzheng et al. [10] designed a 7.5 kW ammonia turbine with an isentropic efficiency of 87% in a one-dimensional design. Through three-dimensional verification, the isentropic efficiency of this structural turbine under design conditions can reach 85%. Yang et al. [11,12] selected five parameters, including evaporation temperature, condensation temperature, temperature difference between evaporator and condenser, and working fluid flow rate, as decision variables for the optimization design of the ocean thermal energy conversion system. This maximizes the net output power per unit area and energy efficiency. They established a simulation model of the ocean thermal energy conversion system using Aspen and MATLAB and proposed corresponding control strategies. The highest cycle thermal efficiency is 3.2%.

In order to further explore the performance of OTEC, relevant experiments have been conducted on the OTEC system. The investment cost of ocean thermal energy conversion power plants is high, and building indoor experimental platforms to conduct simulation research experiments is an effective means to reduce research costs and shorten research and development cycles. There are currently three indoor experimental platforms reported, located at the First Institute of Oceanography of the Ministry of Natural Resources of China, Reunion Island in France, and Saga University in Japan [13–15]. The First Institute of Oceanography of the Ministry of Natural Resources of China has established a 15 kW indoor experimental platform [13,16,17], using the complete Rankine cycle with pure ammonia as the working fluid. The laboratory uses room temperature water as the cold source and high-temperature gas as the heat source to heat seawater. However, the simulated temperatures of surface seawater and deep seawater used in the experiment are both higher than the actual sea conditions [13,18]. France has built an ocean thermal energy test prototype with an equal power of 15 kW on the island of Reunion [14,19]. The working fluid is ammonia, and the cycle structure is the Rankine cycle, which is a 1/250 scaled model of its planned 10 MW thermal energy power plant. The 30 kW indoor experimental platform built by Saga University in Japan [15] adopts a high-performance Uehara cycle structure and is equipped with a deep seawater comprehensive utilization module, including 10 t/day seawater desalination equipment, hydrogen manufacturing and storage equipment, lithium recovery basic experimental equipment, etc., which are of great significance for promoting in-depth research on deep seawater comprehensive utilization technology. Alexandre et al. [20] used the moving boundary method to dynamically model a full liquid evaporator and tested it on a 15 kW ocean thermal energy conversion power generation experimental platform on the island of Reunion. The predicted results of the dynamic model were in good agreement with the experimental results.

Although there are few experimental platforms for OTEC, researchers have made significant progress in ORC experiments. Dong et al. [21] demonstrated, through experiments, the impact of expander speed on ORC system performance under variable operating conditions. Jin et al. [22] studied the effect of external loads on the performance of a 3 kw ORC experimental system. Zhang et al. [23] conducted experimental research on the matching characteristics of ORC operating parameters, indicating that the net output power shows an increasing trend with the increase of engine load. Shao et al. [24] conducted experimental research on the performance and characteristics of kilowatt level ORC systems and tested power generation systems under different cooling conditions. It was found that the mass flow rate of cold water has a significant impact on the operating status of the system and turbine. Li Jifei et al. [25] conducted an experimental study on the impact of changes in heat source conditions on the operating characteristics of organic Rankine cycle units. The stability time of organic Rankine cycle units after the flow step is much shorter than that of the temperature step. Feng Yongqiang et al. [26] obtained 950 sets of experimental data using a 3 kW ORC test bench and established a performance prediction model using reverse neural network principles. The net output power prediction error was only 0.03 kW–0.04 Kw. Guo Yanan et al. [27] built an ORC system experimental setup using R245fa as the working fluid. The author analyzed the influence of temperature, pressure, and speed on the output power, temperature drop, efficiency, and other parameters of the turbine. Zhang et al. [28] compared the efficiency of ORC systems with rated powers of 3 kW and 10 kW through experiments, focusing on the effects of heat sources and radiators. The experiments showed that ORC systems with higher rated power were more optimal. Hijriawan et al. [29] investigated the effect of different motor frequencies on the ORC system of R134a with a turbo expander.

In the field of thermal energy utilization, many people have conducted research on predicting unknown and unmeasured data and obtaining optimal operating parameters. Most of the predictions are based on Rankine cycles, as machine learning methods are receiving increasing attention in ORC. Artificial neural network technology (ANN) is widely used to establish prediction models due to its self-learning, nonlinear, and arbitrary function approximation capabilities [26]. Oguz Arslan [30] used ANN to optimize the supercritical ORC-binary system and pointed out that Levenberg Marguardt (LM) is the best algorithm applied to the system. Xianglong Luo [31] developed a performance prediction method based on artificial neural networks and proposed a systematic method for quickly evaluating ORC performance using existing or new fluids. Fubin Yang et al. [32] established a neural network-based ORC system prediction model, studied the impact of seven key operating parameters on the power output of the ORC system, and conducted performance prediction and parameter optimization for the ORC system. Rushdie et al. [33] proposed a program that combines artificial neural networks and artificial bee colonies (ABC) to optimize the Rankine cycle. Davide Ziviani [34] proposed an artificial neural network modeling method in the ORC system to achieve higher precision mapping extender performance for system simulation. Laura Palagi [35] proposed an optimization model for the multi-objective optimization of small organic Rankine cycles based on a neural network proxy model, which is suitable for solving highly nonlinear constrained optimization problems in typical energy system designs. Mohammad Ali Emadi [36] applied genetic algorithms and artificial neural networks to the multi-objective optimization of new multi-generation systems. Wang et al. [37] proposed an integrated method for reasonable real-time machine learning in ORC research, comparing the ORC prediction models of backpropagation neural networks (BP) and support vector regression (SVR). Through training, rapid prediction of system efficiency was achieved. Peng et al. [38] used an artificial neural network based on the REFPROP computational database to model the thermodynamic processes of over a hundred working fluids, aiming to predict the properties of basic ORC (BORC) and regenerative ORC (RORC) using machine learning methods. Chen et al. [39] reduced the complexity of the system by establishing a high-precision artificial neural network model to predict the pressure drop of the system.

Looking back at previous research, artificial neural network technology has mainly been used to reduce modeling time and save computational costs. On this basis, many people have explored the integration of neural networks and ORC. However, due to the lack of experimental platforms, small temperature differences in simulated seawater changes, and small differences between data in the OTEC cycle, the prediction effect of establishing a neural network is not ideal. In order to achieve accurate prediction and optimization of the performance of the ocean thermal difference energy experimental platform, based on the 50 kW ocean thermal difference energy experimental platform built by the research group, this article established an improved GBO model using 213 sets of experimental data, improved the original backpropagation neural network, and wrote a program method to automatically determine the number of hidden layer nodes. Through the Bayesian hyperparameter optimization method, the optimal hyperparameters were obtained, and a prediction model suitable for the ocean thermal energy conversion experimental platform was established to achieve accurate prediction of performance parameters such as grid-connected power. The multi-objective optimization of turbine grid-connected power and isentropic efficiency was completed, providing a theoretical basis and data guidance for the stable operation and intelligent control of the ocean thermal gradient energy platform.

2. Materials and Methods

2.1. Description of the Test Bench

Figure 1 is a schematic diagram of a 50 kW OTEC experimental prototype. The principle of power generation is that warm seawater exchanges heat with the circulating working fluid in the evaporator, causing the circulating working fluid to transform from a liquid state to a high-pressure gas state. The turbine starts generating electricity under the pressure, and the exhausted gas flowing through the turbine enters the condenser to exchange heat with cold seawater and is pressurized by the working fluid pump in a liquid state for the next cycle. This 50 kW ocean thermal energy conversion experimental platform is currently the most powerful ocean thermal energy conversion experimental platform. Unlike traditional OTEC experimental platforms, it can achieve free regulation of temperature, fully simulate real seawater temperature, and directly conduct sea trials. Figure 2 shows the 50 kW prototype of ocean thermal energy conversion power generation. According to the annual variation of surface seawater temperature in the South China Sea in 2016 as shown in Table 1, the operating temperature range required for the experimental test platform is as follows: cold source 4 °C and heat source 25–30 °C. The lower the temperature of the heat source, the greater the heat exchange required between the evaporator and condenser, and the greater the mass flow of the working medium and cold water. The experimental prototype consists of three parts, namely the warm water circuit, the dual-turbine OTEC circuit, and the cold water circuit. The working fluid is R134a, and the key component parameters are designed according to the design method of a heat source of 28 °C and a cold source of 4 °C. The ideal structural working fluid cycle temperature–entropy change values are shown in Table 2.

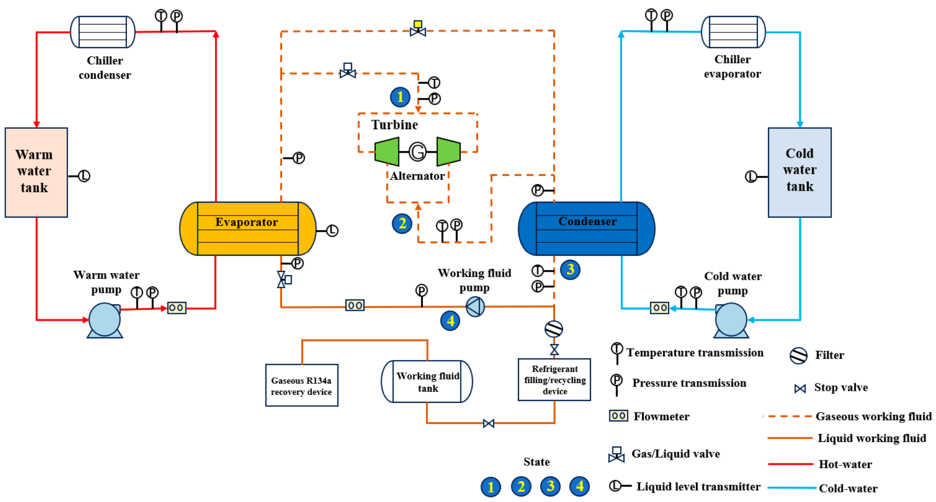

Figure 1. Schematic diagram of a 50 kW OTEC experimental prototype.

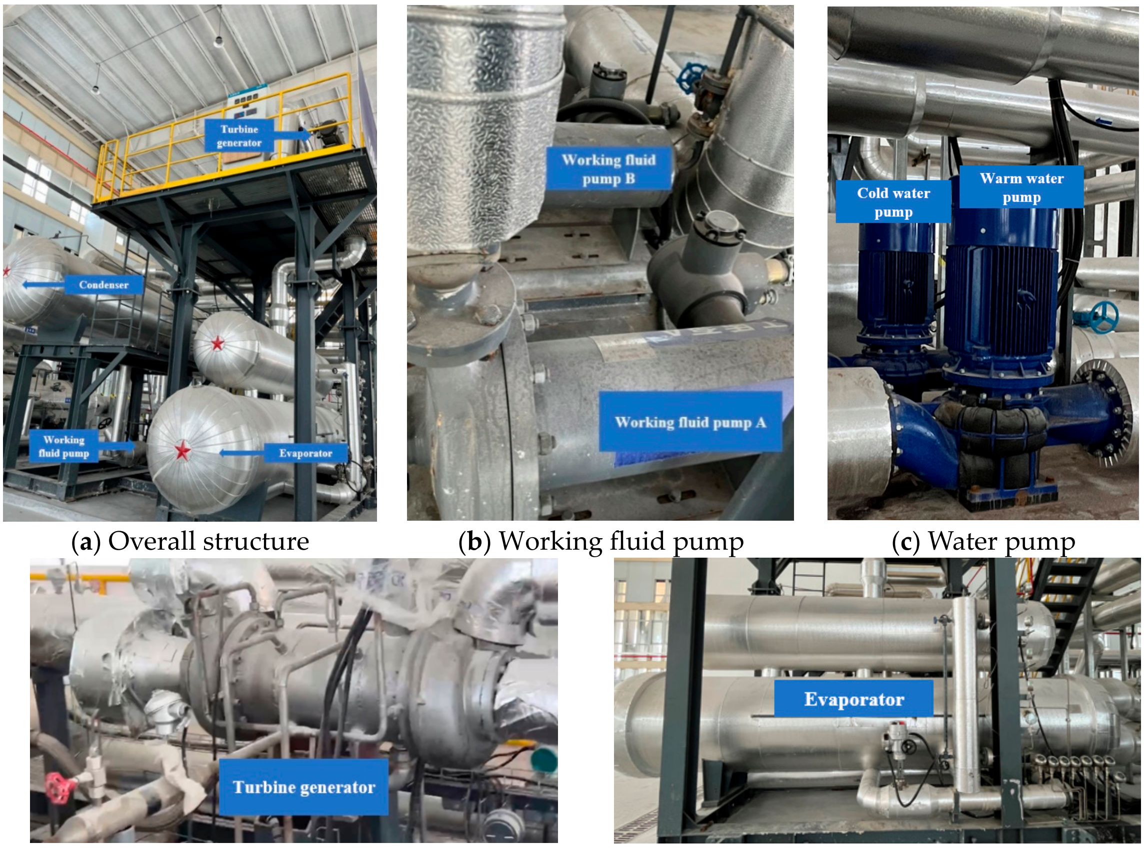

(**a**) Overall structure (**b**) Working fluid pump (**c**) Water pump

(**d**) Turbine generator (**e**) Evaporator

Figure 2. 50 kW ocean thermal energy conversion power generation prototype.

Table 1. Annual variation of surface seawater temperature in the South China Sea in 2016.

Month	Temperature/°C	Month	Temperature/°C	Month	Temperature/°C
1	25	5	29.7	9	29.1
2	24.6	6	30.1	10	28.8
3	25.6	7	29.9	11	27.8
4	27.9	8	29.5	12	26.4

Table 2. Ideal structural working fluid cyclic temperature entropy change value.

State	Temperature (°C)	Pressure (kPa)	Density (kg/m^3)	Specific Enthalphy (kJ/kg)	Specific Entropy (kJ/kg·K)
1	24	645.78	31.389	411.82	1.7166
2	7.999	387.61	19.115	401.39	1.7166
2′	7.999	387.61	18.961	402.95	1.7222
3	8	387.61	1267.9	210.84	1.0388
4	8.1070	645.78	1268.6	211.03	1.0388

2.1.1. Warm and Cold Water Circuits

The warm and cold water circuits of this experimental prototype are mainly controlled by two coordinated units, namely an air-cooled heat pump unit (with an auxiliary water pump) and a water source heat pump unit. Their function is to heat the 26 °C warm water output by the evaporator in the ocean temperature difference energy circulation system to 28 °C, and cool the 6 °C cold water output by the condenser to 4 °C. The warm and cold water, after reaching a certain temperature, enter the warm and cold water tanks, respectively. The warm water enters the evaporator through the warm water pump, and the cold water enters the condenser through the cold water pump, achieving the simulation of the actual temperature difference between warm surface seawater and deep cold seawater.

The mass flow calculation formula for warm and cold water is shown in Equations (1) and (2), and the key parameters are shown in Table 3.

Table 3. Key parameters of warm and cold water circuits.

Parameter		Value	Unit
Warm water pump	Mass flow	191.5	kg/s
	Temperature	28	°C
Cold water pump	Mass flow	184	kg/s
	Temperature	4	°C
Warm water insulation water tank	Volume	30	m^3
Cold water insulation water tank	Volume	30	m^3

Warm water quality flow rate:

$$m_w = \frac{Q_{eva}}{c_w \times (T_{wi} - T_{wo})} \tag{1}$$

Cold water quality flow rate:

$$m_c = \frac{Q_{con}}{c_c \times (T_{co} - T_{ci})} \tag{2}$$

where Q is the heat absorption, T is the inlet and outlet temperature, and c is the specific heat capacity.

2.1.2. Dual Turbine OTEC Circuit

The dual turbine OTEC circuit mainly includes an evaporator, condenser, turbine, working fluid pump, and working fluid pipe. Both the evaporator and condenser are equipped with full liquid heat exchangers, among which the twin turbine generator is a direct drive permanent magnet synchronous generator set, using air floating bearings. The relevant parameters are calculated in Equations (3)–(8), and the key parameters are shown in Table 4. The cyclic theoretical efficiency of the system is as follows:

$$\eta_0 = \frac{(h_1 - h_2) - (h_4 - h_3)}{h_1 - h_4} \tag{3}$$

R134a cycle mass flow rate:

$$m_f = \frac{Q_{eva}}{h_1 - h_4} = \frac{50/\eta_0\eta_t\eta_m}{h_1 - h_4} \tag{4}$$

where $\eta_t = 85\%, \eta_m = 90\%, \eta_p = 60\%$.

Evaporator absorbs heat:

$$Q_{eva} = m_f(h_1 - h_4) \tag{5}$$

Condenser heat dissipation:

$$Q_{con} = m_f(h_2 - h_3) \tag{6}$$

Turbine shaft power:

$$W_t = \eta_t \times m_f(h_1 - h_2) \tag{7}$$

Turbine grid connected power:

$$W_{net} = 0.9W_t \tag{8}$$

Table 4. Key parameters of dual turbine OTEC circuit.

Parameter		Value	Unit
Evaporator	Heat exchange	1608.56	kW
	Evaporation temperature	24	°C
	Evaporation pressure	645.78	kPa
	Warm water mass flow rate	191.5	kg/s
Condenser	Heat exchange	1545.68	kW
	Condensation temperature	8	°C
	Condensation pressure	387.61	kPa
	Cold water mass flow rate	184	kg/s
Working fluid pump	Working fluid mass flow rate	8	kg/s
	Operating temperature	7.9	°C
	Inlet pressure	384.86	kPa
	Outlet pressure	650.99	kPa
Turbine	Inlet temperature	24	°C
	Inlet pressure	632.23	kPa
	Outlet temperature	9	°C
	Outlet pressure	393.96	kPa

2.2. Measurement Device and Operating Method

The measurements in this experiment mainly include temperature, pressure, flow rate, and rotational speed. Temperature transmitters, pressure transmitters, flow transmitters, liquid level transmitters, and speed transmitters were used, respectively. The relevant transmitters were calibrated for experimental errors before the experiment, and all were within the acceptable range. The specifications and parameters are shown in Table 5.

Table 5. Transmitter specification parameters.

Instrument Name	Specification Parameters
Temperature transmitter	accuracy class: A-level ±(0.15 + 0.002∣t∣) °C; −50~200 °C
Pressure transmitter	accuracy class: ±0.1%; −0.1~1.6 Mpa
Flow transmitter	accuracy class: ±0.5%
Speed transmitter	accuracy class: ±0.2%

Temperature and pressure transmitters are placed at the inlet and outlet of the turbine, respectively, and a speed transmitter is installed at the airfoil bearing to measure the turbine speed. The data is uploaded to the control cabinet to achieve signal data acquisition and detection functions. The generator is connected to the grid cabinet through a three-phase rectifier and uploads data to the experimental testing platform, allowing direct reading of the grid power.

In practical experiments, the turbine generator, as the most important component of OTEC, has three important evaluation indicators: grid-connected power, isentropic efficiency, and rotational speed. Grid-connected power can measure the power generation capacity of the experimental test platform, isentropic efficiency can measure the power generation state of the turbine, and rotational speed can monitor the state of the turbine and air bearing in real time. Among them, the grid-connected power and rotational speed of the turbine motor can be directly measured, while the isentropic efficiency needs to be calculated. The calculation formula is shown in Equation (9), where ΔH_{act} is the actual enthalpy drop of the turbine, and ΔH_{ise} is the isentropic enthalpy drop of the turbine.

$$\eta_{tur} = \frac{\Delta H_{act}}{\Delta H_{ise}} \tag{9}$$

When the initial temperature reaches the specified operating conditions of 28 °C and 4 °C, the bypass valve is closed and the turbine inlet valve is gradually opened. After the turbine inlet opening reaches 100%, the experimental data are recorded every 1 s and allowed to run stably for 35 min. The recording is then terminated. A total of 2113 data points are recorded, and a test point is taken every 10 s. This study ultimately selected 213 test points for training and testing ANNs. The parameters of these test points are shown in Table 6.

Table 6. Test point parameters.

Test Point	m_w (m^3/h)	m_c (m^3/h)	$T_{tur,in}$ (°C)	$P_{tur,in}$ (bar)	$T_{tur,out}$ (°C)	$P_{tur,out}$ (bar)	m_f (kg/s)	W_{net} (kW)	η_{tur}	n_{tur} (rpm)
1	648.000	559.51	22.27286	4.71991	12.86531	3.19965	6.782315	30.00000	0.80288	9389.46777
2	720.49	558.07	22.25116	4.72512	12.64106	3.20197	6.567218	30.10000	0.83069	9389.46777
3	738.37	556.77	22.24031	4.75232	12.71340	3.20544	6.895445	30.70000	0.79951	9382.23340
...			...	...	...	...	...	...		
211	825.35	807.86	24.02705	5.05671	12.10576	3.14120	7.389667	41.50000	0.83746	10,264.75684
212	822.53	823.22	24.01982	5.04688	12.08044	3.14120	7.292357	41.30000	0.84615	10,275.60742
213	822.23	825.61	24.02344	5.05035	12.15278	3.14410	7.374606	41.30000	0.83812	10,384.11523

2.3. Algorithm Model

2.3.1. GA-BP Neural Network

A BP neural network is a multi-layer feedforward neural network, which was described and analyzed in detail by Rumelhart and McClelland in a book in 1986 [40]. The commonly used three-layer structure is the input layer, hidden layer, and output layer. The basic idea of BP neural network learning and training is to continuously modify the weights and thresholds of the network under given input and output information, so that the network can achieve the given input–output mapping relationship.

After determining the structure of the BP neural network, the initial weights and thresholds are randomly generated, but they have a significant impact on the convergence speed and prediction accuracy of the network and cannot be accurately obtained. In response to this, the genetic algorithm can be used to minimize prediction error, with initial weights and thresholds as design variables to find the optimal weights and thresholds. The obtained optimal weights and thresholds can be used as weights and thresholds for the BP neural network. This not only enables network training to have faster convergence speed but also better prediction accuracy.

Set the initial population size to gen_num, calculate the fitness function of each population, select chromosomes with higher fitness through roulette wheel gambling, and form a new population for the next iteration after crossing and mutation. The equation can be expressed as follows:

$$f(x) = Tansig(x) = \frac{e^x - e^{-x}}{e^x + e^{-x}}, f(x) \in (0,1) \tag{10}$$

$$A_1 = Tansig(W_1 \times X + b_1) \tag{11}$$

$$\hat{y} = W_2 \times A_1 + b_2 \tag{12}$$

$$fitness = (\hat{y} - y)^2 \tag{13}$$

Let the input data be X, if it is true, the output is y, and after model prediction, the output is $\hat{y}$, W_1 is the weight matrix connecting the input layer and the hidden layer, b_1 is the deviation between the connection input layer and the output layer, W_2 is the weight matrix connecting the output layer and the hidden layer, and b_2 is the deviation between connecting the output layer and the hidden layer.

2.3.2. GP-BP-OTEC Neural Network

The input layer of the GA-BP neural network selects seven parameters as input layer parameters, including turbine inlet temperature and pressure, turbine outlet temperature and pressure, temperature and cold water mass flow, and working medium mass flow. The turbine grid-connected power, isentropic efficiency, and turbine speed are used as output layer parameters to construct a single hidden-layer GP-BP-OTEC model. The GP-BP-OTEC (GBO) neural network flowchart is shown in Figure 3. Among them, the number of hidden layer nodes has a significant impact on the prediction accuracy of neural network prediction, and in the subsequent parameter selection process, if the number of hidden layer nodes is considered, it will become more complex. Therefore, this article determines the number of hidden layer nodes before parameter selection to reduce the complexity of the model and improve its accuracy. The network model diagram and its pseudo-code are shown in Figure 4.

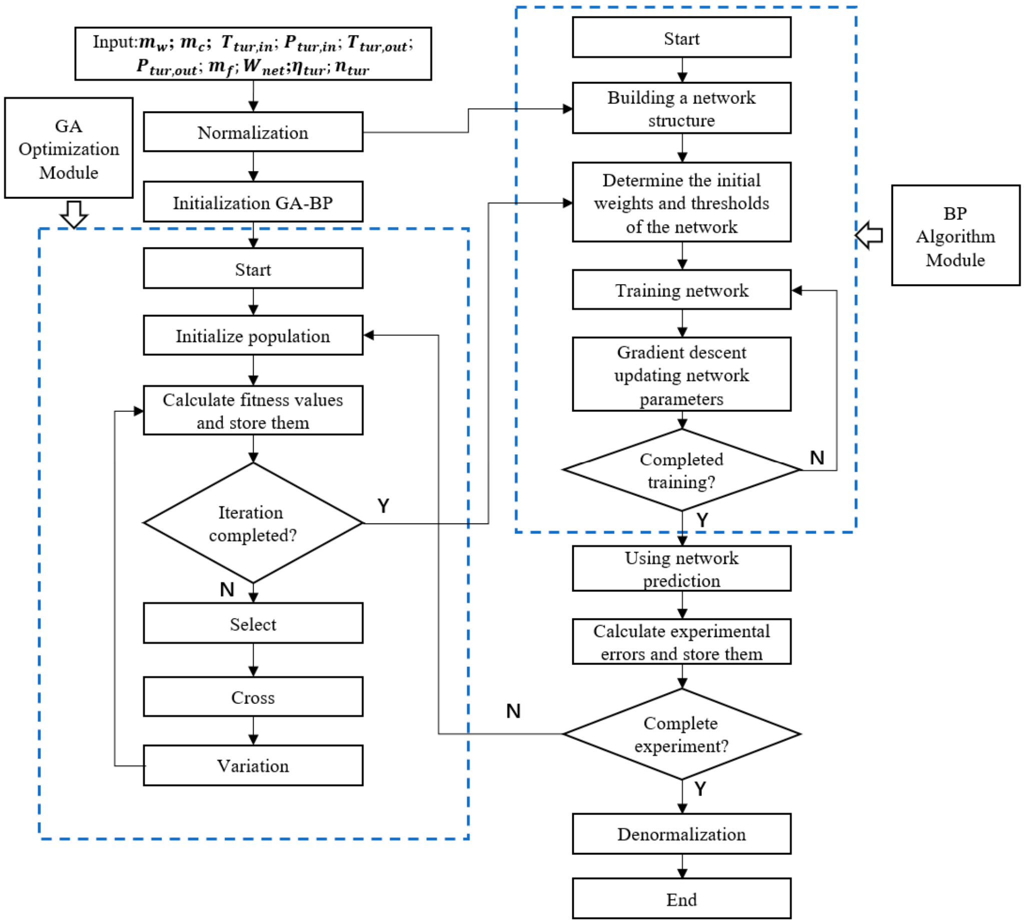

Figure 3. GP-BP-OTEC neural network flow chart.

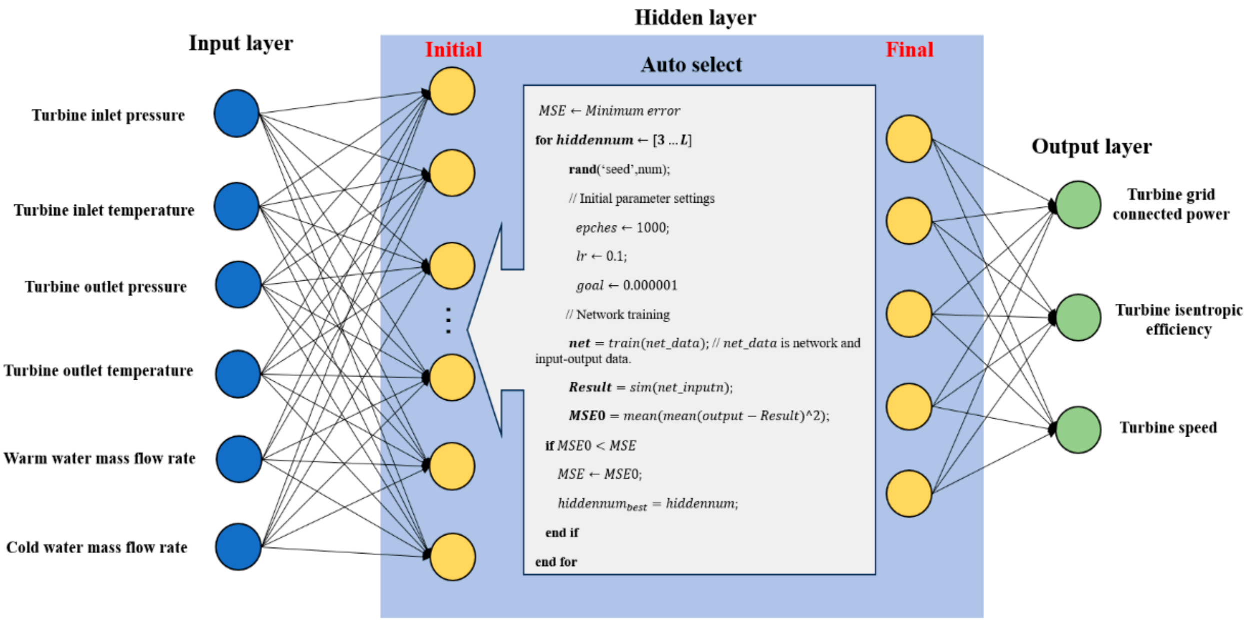

Figure 4. Network model diagram and pseudocode.

2.3.3. GBO Neural Network Model Evaluation Indicators

When evaluating GBO, mean square error (MSE), goodness of fit (R^2), and mean absolute percentage error ($MAPE$) are selected as evaluation indicators. The smaller the MSE value and the closer the $MAPE$ value is to 0, the higher the model accuracy. The closer the R^2 value is to 1, the higher the model fit. The equations for MSE, R^2, and $MAPE$ are expressed as follows:

$$MSE = \frac{1}{Q}\sum_{k=1}^{Q}[y(k) - t(k)]^2 \tag{14}$$

$$R^2 = 1 - \frac{\sum_k [y(k) - t(k)]^2}{\sum_k [t - t(k)]^2} \tag{15}$$

$$MAPE = \frac{100\%}{Q}\sum_{k=1}^{Q}\left|\frac{y(k) - t(k)}{t(k)}\right| \tag{16}$$

Among them, $y(k)$ is the predicted value, and $t(k)$ is the actual experimental data; y and t are the average values of the predicted and experimental data, respectively.

3. Results and Discussion

3.1. Experimental Data Analysis

In order to better understand the operation of the OTEC system, this section mainly analyzes the mutual influence between system parameters and system evaluation indicators. The mass flow rates of warm and cold water and working fluid are measured by flow transmitters, and the turbine inlet and outlet temperatures, pressures, grid-connected power, speed, and isentropic efficiency of the turbine are calculated as shown in Section 3.2.

Figures 5–7 show the changes in the experimental process over time. The changes in system parameters are shown in Figure 5. After about 700 s, the experiment basically entered a stable operating state, with the mass flow rate of warm water maintained at 750 m^3/h and the mass flow rate of cold seawater maintained at 730 m^3/h. The turbine inlet temperature gradually increased over time, while the turbine inlet pressure also increased, indicating a positive correlation between turbine inlet temperature and pressure. The turbine outlet temperature first decreased and then increased, while the turbine outlet pressure showed the same trend.

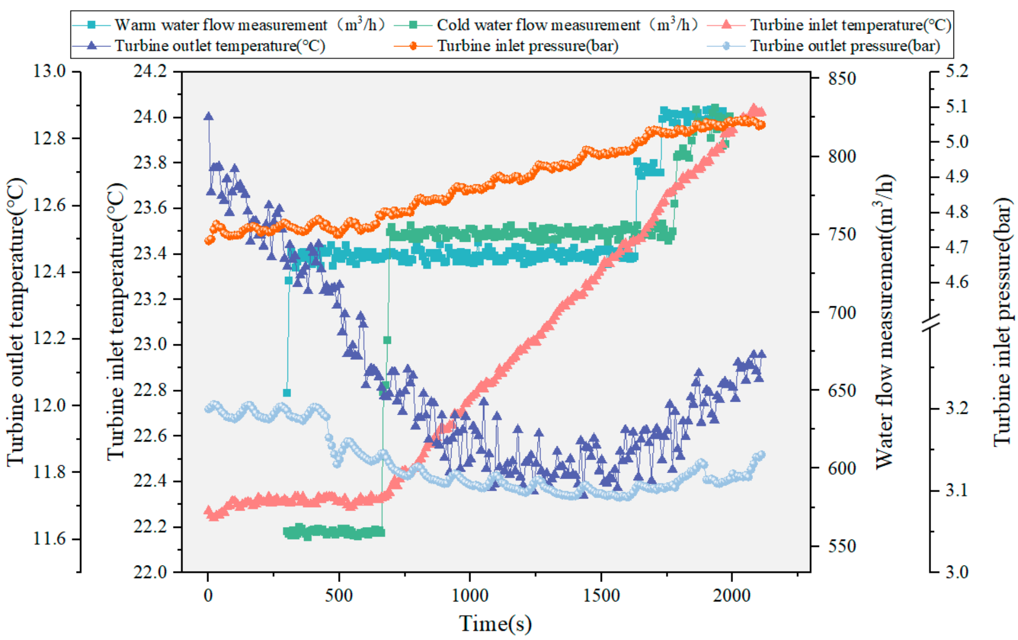

Figure 5. Changes in system parameters.

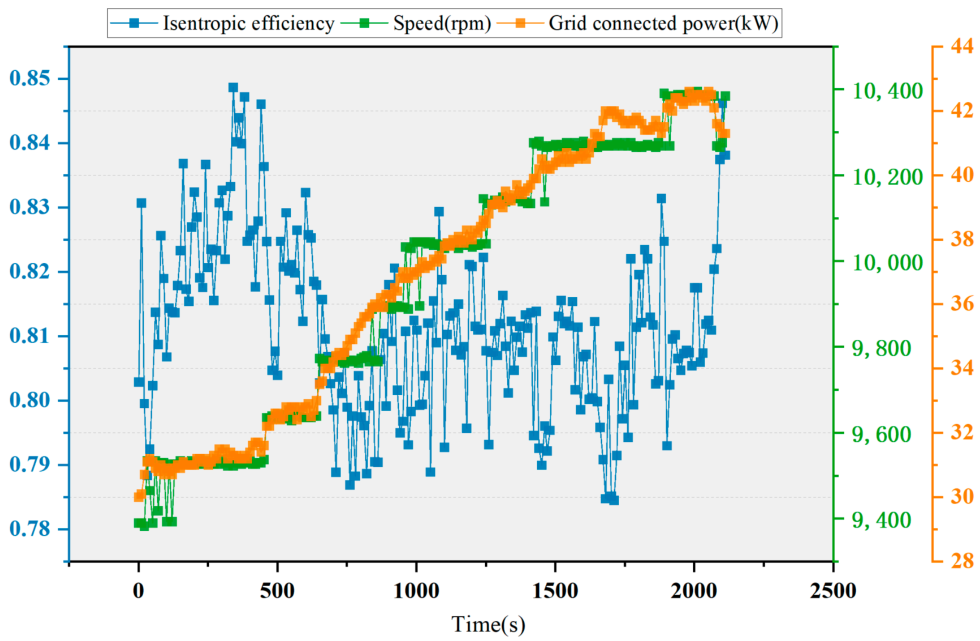

Figure 6. System evaluation parameter changes.

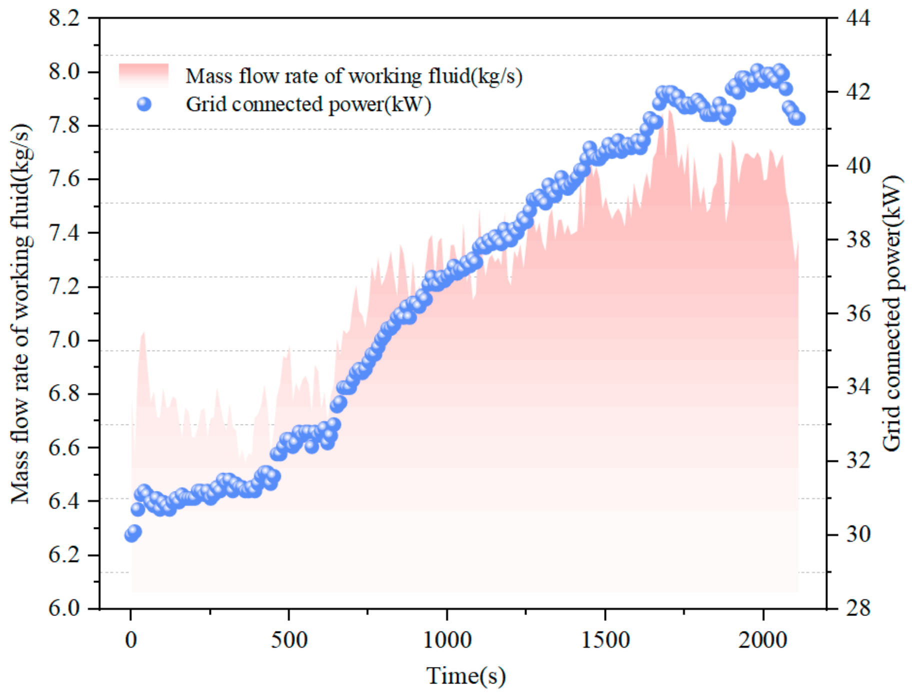

Figure 7. Relationship between quality flow and grid-connected power.

Figure 6 shows the changes in three evaluation indicators. It can be seen that the turbine grid-connected power is positively correlated with the speed. As the experiment begins, the turbine grid-connected power shows an upward trend. When the experiment proceeds to about 1000 s–1500 s, only the turbine inlet temperature rises, while the turbine outlet temperature remains basically unchanged. Therefore, the turbine inlet temperature, pressure, and power are positively correlated. At around 1500 s–1600 s, the turbine outlet temperature rises, and the trend of turbine output power increases slowly. From the above, it can be concluded that the turbine outlet temperature pressure and output power are negatively correlated, and the change in turbine inlet temperature has a greater impact on the system. The mass flow of warm water increases around 1600 s–1700 s, while the temperature of cold water remains basically unchanged. The inlet temperature of the turbine also increases in the same trend, and the increase in turbine power becomes larger; From 1850 s to 2000 s, as the mass flow rate of cold water increases, the temperature of both warm and cold water remains relatively constant. The inlet temperature of the turbine follows a similar trend, and the increase in turbine power is also greater. Therefore, there is a positive correlation between the temperature of warm and cold water and the output power of the turbine. In summary, there is an interactive relationship between the parameters of each system and the output indicators.

As shown in Figure 7, the change trend of the mass flow rate of the working medium is basically consistent with the change trend of the turbine grid-connected power, but the isentropic efficiency does not have a consistent change trend with a certain parameter, which should be affected by comprehensive parameters. Using the Relieff algorithm for feature selection and single-objective prediction, the results are shown in Figure 8. All parameters are correlated with the isentropic efficiency, and the mass flow rate has the greatest impact on it. If the number of retained features is changed, it can be found that the R^2 value decreases significantly. Therefore, these parameters must be selected as input data.

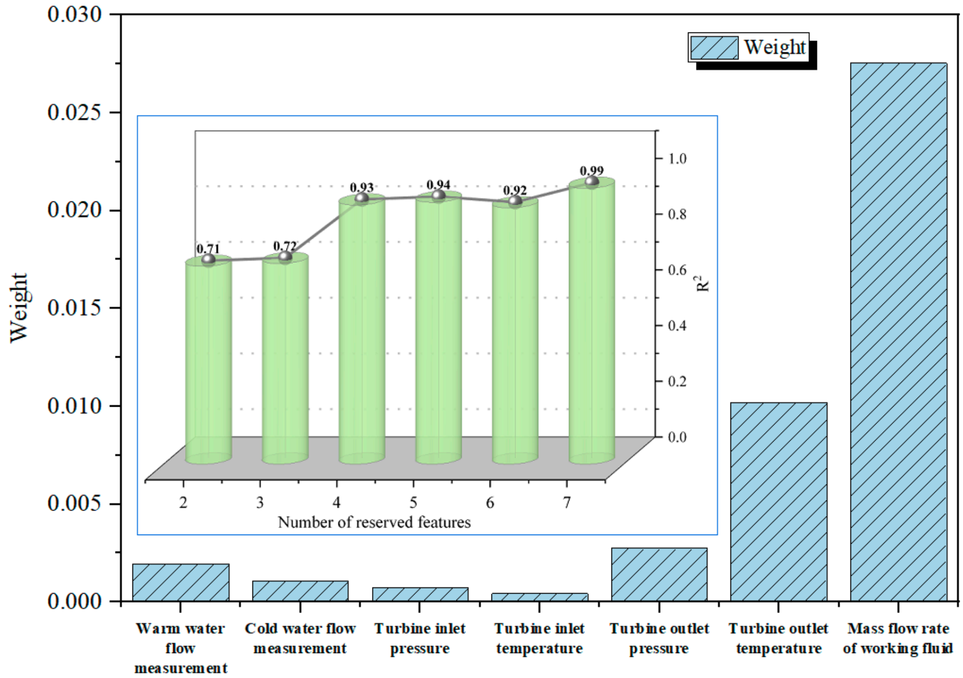

Figure 8. Feature selection.

3.2. GBO Model Analysis

After establishing the GBO model, it is necessary to set its parameters and training functions to improve the accuracy of prediction. The parameters that need to be determined include the learning rate, initial population size, crossover probability, and mutation probability. The ratio of training set to testing set used in this article is 8:2, with 40 sets of testing sets randomly selected for analysis. Additionally, the BP neural network comes with a built-in validation function, eliminating the need for setting a separate validation set.

3.2.1. The Impact of the Training Function on the GBO Neural Network

According to previous research, different training functions use different training algorithms, resulting in significant differences in the prediction results of network models. This article selects five different training functions ('trainlm', 'trained', 'traingdm', 'trainrp', 'traincgb'). Traind is a common gradient descent method that adjusts the weights and thresholds of the network along the negative gradient direction of the network performance parameters. Traingdm represents a gradient descent algorithm with momentum, which is also a batch processing feedforward neural network training method. It not only has faster convergence speed but also introduces a momentum term, effectively avoiding the occurrence of local minimum problems in network training. Trainrp is a rebound BP algorithm used to eliminate the impact of the gradient modulus on network training and improve training speed. Traincgb uses the Plwell–Beale algorithm to determine whether the adjustment direction of weights and thresholds returns to the negative gradient direction by judging the orthogonality of the front and back gradients. Trainlm is one of the most popular algorithms in BP neural networks, using Levenberg–Marquardt backpropagation.

From Figure 9, it can be seen that the R^2 values using trainlm are the highest, at 0.996, 0.9979, and 0.9858, respectively, while the R^2 values using trainrp and traincgb are basically the same.

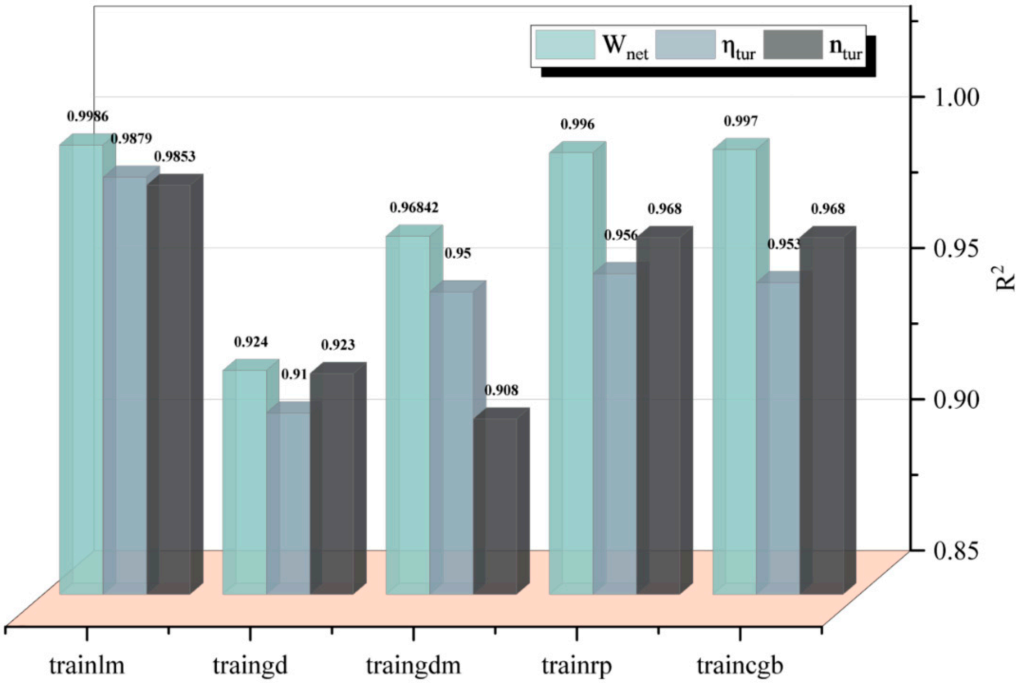

Figure 9. The impact of training functions on model accuracy.

3.2.2. Initial Parameter Selection

During the parameter adjustment process of neural networks, it is common to manually adjust the above training parameters for repeated training to select the optimal parameters. However, there are some problems. First, the training time is too long. Second, because the neural network training process is a complex superimposed process, it is not very accurate or judge whether the composite conditions are optimal by changing only a single parameter. Therefore, this article chooses to use a Bayesian optimizer to optimize the GBO neural network algorithm to find the optimal parameter values to construct a regression model. The Bayesian optimizer is a black-box optimizer used to find optimal parameters. The algorithm has a large number of continuous parameters in the parameter space and has a relatively short running time. The initial parameter set and the optimization range of the hyperparameters involved in the algorithm are shown in Table 7. The selection and range of the hyperparameters are empirically selected.

Table 7. Hyperparameter optimization range.

Parameters	Initial	Min	Max
Learning rate	0.1	0.01	0.8
Population size	50	30	120
Crossover probability	0.8	0.6	0.9
Mutation probability	0.02	0.01	0.2

From Figure 10, it can be seen that the R^2 of the optimized model has been improved, with the maximum output power R^2 of the turbine reaching 0.99942, the isentropic efficiency R^2 of the turbine being 0.99906, and the speed R^2 of the turbine being 0.98764. All three output parameters have good fitting goodness. The final parameter values for the model are shown in Table 8.

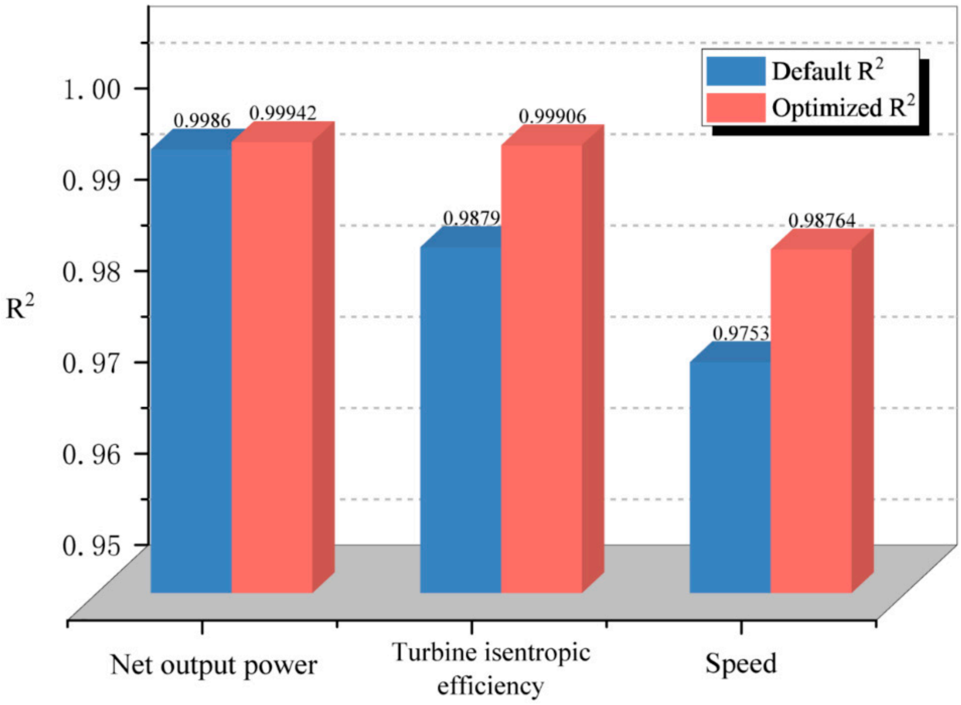

Figure 10. Hyperparameter optimization results.

Table 8. Final parameter selection for the GBO.

Parameters	Value
Learning rate	0.1
Train function	trainlm
Population	70
Number of hidden layer nodes	10
Crossover probability	0.8
Mutation probability	0.2
Training precision	0.00001
Hidden layer function	tansig
Output layer function	purelin

3.3. Model Accuracy Prediction and Evaluation

The grid-connected power, isentropic efficiency, and rotational speed of 40 groups of turbines were predicted, respectively. The prediction results and their errors of the turbine grid-connected power are shown in Figure 11. It can be seen that the true values and the predicted values are basically fitted, with a mean square error (MSE) of 0.010633, a maximum error of 0.246 kW, and an average absolute percentage error ($MAPE$) of 0.24547%.

The prediction results and errors of the isentropic efficiency of the permeability are shown in Figure 12. It can be seen that the true values and predicted values are basically fitted, with a MSE value of 1.9168×10^{-7}, a maximum error of 0.00135, and an $MAPE$ of 0.04%.

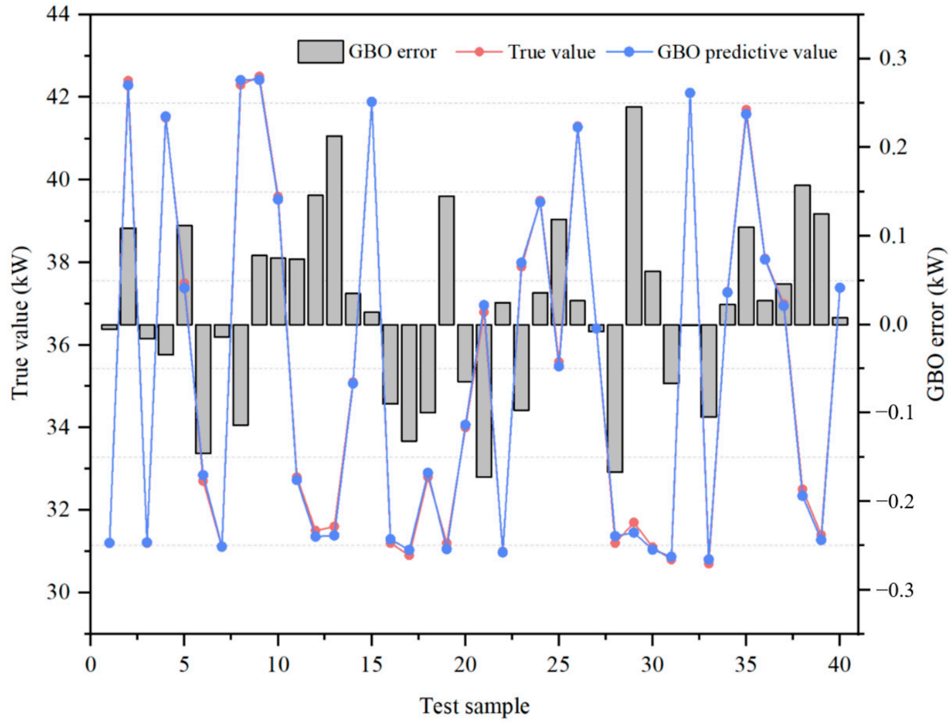

Figure 11. Prediction results and errors of turbine grid connected power.

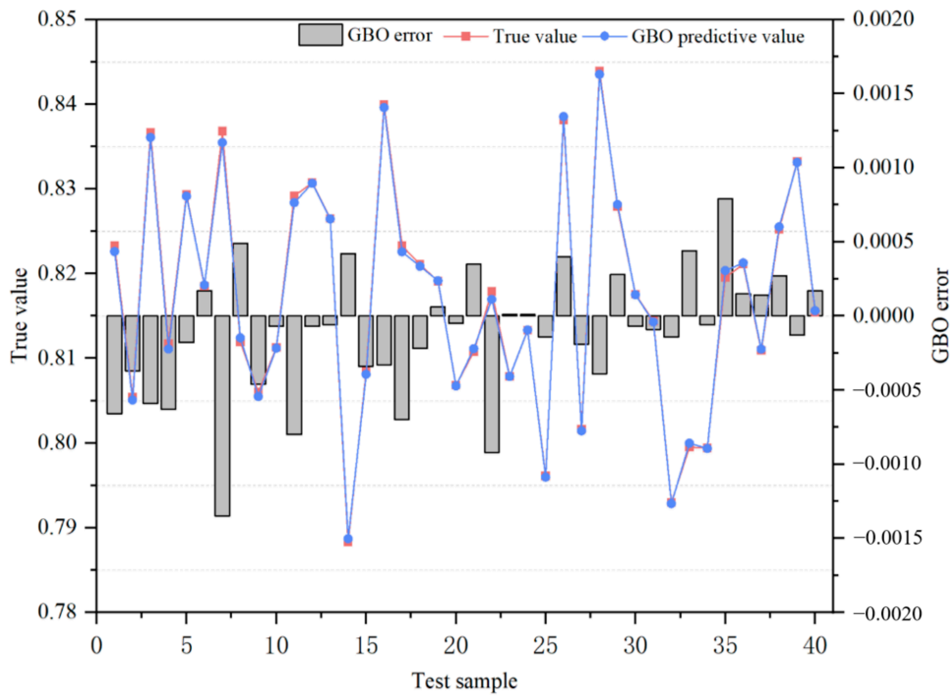

Figure 12. Prediction results and errors of isentropic efficiency of turbine.

The prediction results and their errors of turbine speed are shown in Figure 13. It can be seen that the real values and the predicted values are basically fitted, except for a small number of data points with deviations. The MSE value is 2050, and the $MAPE$ is 0.33%. The reason for the large MSE value is that the speed itself has a large base, basically at 10,000 rpm, so the mean square error will also be large, but its maximum error is only 121 rpm, which is 1% of the actual data, so it meets the experimental prediction requirements.

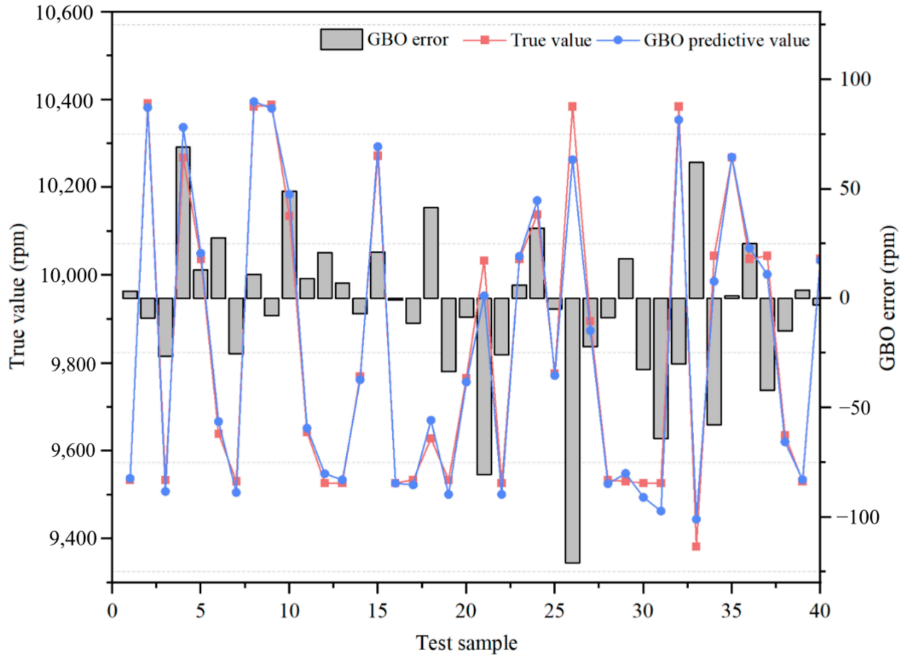

Figure 13. Prediction results and errors of turbine speed.

3.4. Multi-Objective Optimization

Based on the analysis of experimental data, it is clear that operating parameters play an important role in the overall system performance. The reasonable selection of operating parameters can effectively improve system performance. As a key component of the experiment, the turbine's power generation effect is crucial. For the system, its turbine grid-connected power and isentropic efficiency are the two most important evaluation indicators. The higher these two indicators are, the better the turbine's power generation effect is. In order to achieve the best results at the same time, this section uses the NSGA-II genetic algorithm to perform multi-objective optimization on two evaluation metrics based on the GBO model. The basic parameters of the NSGA-II are shown in Table 9. Since this article uses air-bearing technology, it is necessary to limit the turbine speed. Considering the energy balance relationship between parameters and the actual experimental data, the constraints shown in Equation (17) need to be met, and the multi-objective optimization expression under design conditions is shown in Equations (18)–(20).

$$T_{tur,in} > T_{tur,out}; P_{tur,in} > P_{tur,out} \tag{17}$$

$$Opt = min\{W_{net}, \eta_{th}\}; n_{tur} \leq 12500 \tag{18}$$

$$\vec{X} = [m_w, m_c, T_{tur,in}, P_{tur,in}, T_{tur,out}, P_{tur,out}, m] \tag{19}$$

$$[600, 600, 22, 4, 11, 3, 6] \leq \vec{X} \leq [800, 800, 24, 5, 13, 4, 8] \tag{20}$$

Table 9. The specific parameter of NSGA-II.

Parameter	Value
Population size	50
Iterations	100
Crossover probability	0.8
Mutation probability	0.1

The Pareto optimization results are shown in Figure 14, where each point represents an optimal situation. It can be seen from the graph that there is no ideal point that maximizes both. In order to select the optimal result, it is necessary to normalize it first, as shown in

Figure 15. The normalization results of two optimization objectives should reach 0.5 or above at the same time, and the two performance schemes are relatively balanced. This article uses the LINMAP method for optimal screening of data. The LINMAP method calculates the distance between each solution and the ideal point (f_{1max}, f_{2max}), and the solution with the smallest distance is the globally optimal solution. The distance between Plan i and the ideal point is given by Equation (21):

$$l_{i+} = \sqrt{(f_{1i} - f_{1max})^2 + (f_{2i} - f_{2max})^2} \tag{21}$$

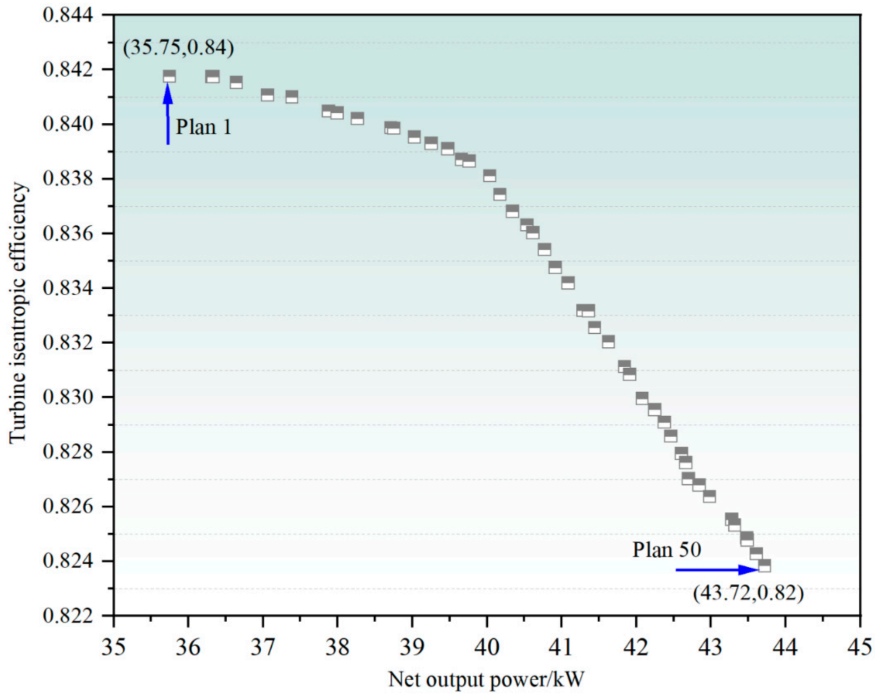

Figure 14. Pareto optimization results.

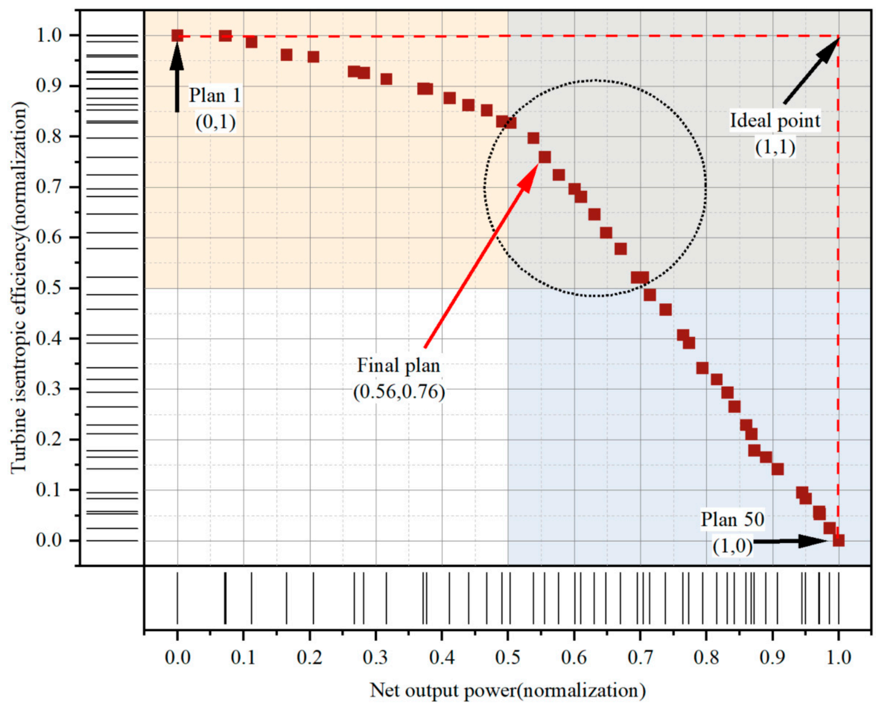

Figure 15. Normalization processing result.

The No. 26 scheme is selected as the final scheme, with the specific parameters shown in Table 10. Under this scheme, the grid-connected power of the turbine is 40.1792 kW, and the isentropic efficiency is 0.837439.

Table 10. Parameters of Scheme No. 26.

Parameter	Numerical Value	Unit
m_w	760.8	m^3/h
m_c	665	m^3/h
$T_{tur,in}$	24	°C
$P_{tur,in}$	5	bar
$T_{tur,out}$	11.01	°C
$P_{tur,out}$	3.14	bar
m	7.95	kg/s
W_{net}	40.1792	kW
η_{tur}	0.83749	

4. Conclusions

This article analyzes the turbine experimental parameters based on 2113 sets of basic experimental data obtained from the 50 kW OTEC experimental platform. Among them, 213 groups were used to establish a GBO model, considering the influence of seven operating parameters including turbine inlet temperature and pressure, turbine outlet temperature and pressure, the mass flow of warm and cold water, and the mass flow of working medium on the turbine grid-connected power, isentropic efficiency, and speed. The optimal output performance was obtained using the NSGA-II genetic algorithm. The results are as follows:

1. The mass flow rate of warm and cold water, the inlet temperature and pressure of the turbine, and the grid-connected power of the turbine are positively correlated. The change in mass flow rate is consistent with the change in turbine output power. The outlet temperature and pressure of the turbine are negatively correlated with the grid-connected power of the turbine; the isentropic efficiency of the permeable is affected by the combined influence of seven operating parameters, all of which are essential, with the mass flow rate of the working fluid having the greatest impact.
2. This article ultimately chooses to use the trainlm training function and uses a Bayesian optimizer to optimize the hyperparameters of the GBO model. The number of hidden layer nodes is automatically determined by an improved BP algorithm, reducing training time and determining the number of hidden layer nodes to be 10;
3. The trained GBO model has good fitting accuracy for the three output parameters, with the maximum R^2 of turbine grid-connected power reaching 0.99942, the R^2 of turbine entropy efficiency reaching 0.99906, and the R^2 of the turbine speed reaching 0.98764. The maximum errors of the three parameters are 0.246 kW, 0.00135, and 121 rpm, respectively, meeting the experimental accuracy requirements;
4. Within a reasonable range of parameter variations, the grid-connected power and isentropic efficiency of the turbine cannot be optimized simultaneously. The Pareto frontier is obtained and normalized, and the optimal result obtained using the LINMAP method is a turbine grid-connected power of 40.1792 kW and an isentropic efficiency of 0.837439.

In summary, this article achieves the accurate prediction of performance parameters such as grid-connected power and completes a multi-objective optimization of turbine grid-connected power and isentropic efficiency, laying the foundation for the study of stable operation and control of ocean temperature difference energy platforms.

Author Contributions: Conceptualization, software, methodology, data curation, writing—original draft preparation and validation, Y.Y.; conceptualization, supervision, and funding acquisition, Y.L.

and M.T.; writing—review and editing, Y.C.; project administration, B.L. All authors contributed to the design of the study. All authors have read and agreed to the published version of the manuscript.

Funding: Thanks to the support provided of the Southern Marine Science and Engineering Guangdong Laboratory (Zhanjiang) Project (ZJW-2019-05) and the fund of Qingdao Human Resources and Social Security Bureau, the Qingdao Postdoctoral Program (QDBSH20230102007).

Data Availability Statement: The original contributions presented in the study are included in the article, and further inquiries can be directed to the corresponding authors.

Conflicts of Interest: The authors declare no conflicts of interest.

Nomenclature

m	Mass flow rate, m^3/h or kg/s	*c*	cold
N	Rotational speed, rpm	*w*	warm
W	Power; kW	*f*	working fluid
p	Pressure, bar	**Acronyms**	
T	Temperature, °C	OTEC	Ocean Thermal Energy Conversion
Subscripts		ANN	Artificial Neural Network
exp	expander	GA	Genetic Algorithm
con	condenser	BP	Back Propagation
tur	turbine	*MSE*	Mean Squared Error
in	inlet	R	Correlation coefficient
out	outlet	*MAPE*	Mean Average Percentage Error

References

1. Zhai, X.Y. Research on Ocean Thermoelectric Power Generation System and Its Heat Exchanger and Ejector. Master's Thesis, Shandong University, Jinan, China, 2021. [CrossRef]
2. Liu, W.M.; Chen, F.Y.; Ge, Y.Z.; Peng, J.P.; Liu, L.; Yang, X.; Song, J.Z.; Liu, K.L. Review of efficiency research on ocean thermal energy systems. *Coast. Eng.* **2022**, *41*, 441–450.
3. Quoilin, S.; Van Den Broek, M.; Declaye, S.; Dewallef, P.; Lemort, V. Techno-economic survey of Organic Rankine Cycle (ORC) systems. *Renew. Sustain. Energy Rev.* **2013**, *22*, 168–186. [CrossRef]
4. Yoon, J.I.; Son, C.H.; Baek, S.M.; Ye, B.H.; Kim, H.J.; Lee, H.S. Performance characteristics of a high-efficiency R717 OTEC power cycle. *Appl. Therm. Eng.* **2014**, *72*, 304–308. [CrossRef]
5. Miljkovic, M. Injection power cycle applied in OTEC power plants. *Energy Procedia* **2017**, *143*, 823–828. [CrossRef]
6. Kalina, A.I. Combined Cycle System with Novel Bottoming Cycle. *ASME J. Eng. Turbines Power* **1984**, *106*, 737–742. [CrossRef]
7. Uehara, H.; Ikegami, Y.; Nishida, T. Performance Analysis of OTEC System Using a Cycle with Absorption and Extraction Processes. *Nihon Kikai Gakkai Ronbunshu B Hen Trans. Jpn. Soc. Mech. Eng. Part B* **1998**, *64*, 2750–2755. [CrossRef]
8. Xue, B. Performance Study of Karina Cycle and Upper Primary Cycle Marine Thermoelectric Power Generation Systems. Master's Thesis, China University of Petroleum, Beijing, China, 2020.
9. Liu, W.M.; Chen, F.Y.; Wang, Y.Q. Progress of Closed-Cycle OTEC and Study of a New Cycle of OTEC. *Adv. Mater. Res.* **2012**, *354–355*, 275–278. [CrossRef]
10. Ge, Y.Z.; Peng, J.P.; Chen, F.Y.; Liu, L.; Liu, W.M. Design and performance impact of marine thermoelectric power generation turbines. *Sci. Technol. Bull.* **2021**, *39*, 96–101.
11. Yang, X.; Liu, Y.; Chen, Y.; Zhang, L. Optimization Design of the Organic Rankine Cycle for an Ocean Thermal Energy Conversion System. *Energies* **2022**, *15*, 6683. [CrossRef]
12. Yang, X.; Liu, Y.; Chen, Y.; Zhang, L. Operation Control and Performance Analysis of an Ocean Thermal Energy Conversion System Based on the Organic Rankine Cycle. *Energies* **2022**, *15*, 3971. [CrossRef]
13. Chen, F.; Liu, L.; Peng, J.; Ge, Y.; Wu, H.; Liu, W. Theoretical and experimental research on the thermal performance of ocean thermal energy conversion system using the rankine cycle mode. *Energy* **2019**, *183*, 497–503. [CrossRef]
14. Martins, M.; Sinama, F.; Lucas, F. Equivalent Gibbs systems for modelling an onshore OTEC experimental plant on Reunion Island. *Int. J. Energy Res.* **2013**, *37*, 1112–1121. [CrossRef]
15. Present Study-Ocean Thermal Energy Conversion | Introduction of Each Division's Researches | Research & Education | Institute of Ocean Energy Saga University Japant [EB/OL]. Available online: https://www.ioes.saga-u.ac.jp/en/research/ioes_present_study/otec_present_study (accessed on 17 September 2022).
16. Chen, F.; Liu, L.; Peng, J. Theoretical analysis and testing of the performance of the Rankine cycle ocean thermoelectric power generation system. *Sci. Technol. Rev.* **2021**, *39*, 90–95.
17. Liu, W. Research and Experimentation on 15 kW Thermoelectric Generator. *China Sci. Technol. Achiev.* **2014**, *1*, 17. [CrossRef]

18. Peng, J.; Wu, H.; Ge, Y.; Chen, F.; Liu, L.; Liu, W. The experimental study of rankine cycle in ocean thermal energy conversion. *Lop Conf. Ser. Mater. Sci. Eng.* **2018**, *381*, 12126. [CrossRef]
19. Journoud, A.; Sinama, F.; Lucas, F. Experimental Ocean Thermal Energy Conversion (OTEC) project on the Reunion Island. In Proceedings of the 4th International Conference on Ocean Energy, Dublin, Irland, 17–19 October 2012.
20. Dijoux, A.; Sinama, F.; Marc, O.; Castaing-Lasvignottes, J. Modelling and experimentation of heat exchangers for Ocean Thermal Energy Conversion during transient operation. *J. Procedia Manuf.* **2019**, *35*, 298–303. [CrossRef]
21. Dong, S.; Hu, X.; Huang, J.F.; Zhu, T.; Zhang, Y.; Li, X. Investigation on improvement potential of ORC system off-design performance by expander speed regulation based on theoretical and experimental exergy-energy analyses. *Energy* **2021**, *220*, 119753. [CrossRef]
22. Jin, Y.L.; Gao, N.P.; Zhu, T. Effect of resistive load characteristics on the performance of Organic Rankine cycle (ORC). *Energy* **2022**, *246*, 123407. [CrossRef]
23. Zhang, X.; Wang, X.; Cai, J.; He, Z.; Tian, H.; Shu, G.; Shi, L. Experimental study on operating parameters matching characteristic of the organic Rankine cycle for engine waste heat recovery. *Energy* **2022**, *244*, 122681. [CrossRef]
24. Shao, L.; Ma, X.; Wei, X.; Hou, Z.; Meng, X. Design and experimental study of a small-sized organic Rankine cycle system under various cooling conditions. *Energy* **2017**, *130*, 236–245. [CrossRef]
25. Li, J.; Li, R.; Miao, Z.; Xu, J. Experimental study on the influence of heat source temperature and flow rate on the operating characteristics of organic Rankine cycle systems. *Therm. Power Gener.* **2022**, *51*, 106–112.
26. Feng, Y.Q.; Liu, Y.Z.; Wang, X.; He, Z.X.; Hung, T.C.; Wang, Q.; Xi, H. Performance prediction and optimization of an organic Rankine cycle (ORC) for waste heat recovery using back propagation neural network. *Energy Convers. Manag.* **2020**, *226*, 113552. [CrossRef]
27. Gou, Y.; Li, L.; Min, H. Design and performance experiment of radial inflow turbine expander for organic Rankine cycle system. *Int. J. Low-Carbon Technol.* **2021**, *16*, 1202–1209. [CrossRef]
28. Zhang, Y.F.; Li, M.J.; Ren, X.; Duan, X.Y.; Wu, C.J.; Xi, H.; Feng, Y.Q.; Gong, L.; Hung, T.C. Effect of heat source supplies on system behaviors of ORCs with different capacities: An experimental comparison between the 3 kW and 10 kW unit. *Energy* **2022**, *254*, 124267. [CrossRef]
29. Hijriawan, M.; Pambudi, N.A.; Wijayanto, D.S.; Biddinika, M.K.; Saw, L.H. Experimental analysis of R134a working fluid on Organic Rankine Cycle (ORC) systems with scroll-expander. *Eng. Sci. Technol.* **2022**, *29*, 101036. [CrossRef]
30. Arslan, O.; Yetik, O. ANN based optimization of supercritical ORC-Binary geothermal power plant: Simav case study. *Appl. Therm. Eng.* **2011**, *31*, 3922–3928. [CrossRef]
31. Luo, X.; Wang, Y.; Liang, J.; Qi, J.; Su, W.; Yang, Z.; Chen, J.; Wang, C.; Chen, Y. Improved correlations for working fluid properties prediction and their application in performance evaluation of sub-critical Organic Rankine Cycle. *Energy* **2019**, *174*, 122–137. [CrossRef]
32. Yang, F.; Cho, H.; Zhang, H.; Zhang, J.; Wu, Y. Artificial neural network (ANN) based prediction and optimization of an organic Rankine cycle (ORC) for diesel engine waste heat recovery. *Energy Convers. Manag.* **2018**, *164*, 15–26. [CrossRef]
33. Rashidi, M.M.; Galanis, N.; Nazari, F.; Parsa, A.B.; Shamekhi, L. Parametric analysis and optimization of regenerative Clausius and organic Rankine cycles with two feedwater heaters using artificial bees colony and artificial neural network. *Energy* **2011**, *36*, 5728–5740. [CrossRef]
34. Ziviani, D.; James, N.A.; Accorsi, F.A.; Braun, J.E.; Groll, E.A. Experimental and numerical analyses of a 5kWe oil-free open-drive scroll expander for small-scale organic Rankine cycle (ORC) applications. *Appl. Energy* **2018**, *230*, 1140–1156. [CrossRef]
35. Palagi, L.; Sciubba, E.; Tocci, L. A neural network approach to the combined multi-objective optimization of the thermodynamic cycle and the radial inflow turbine for Organic Rankine cycle applications. *Appl. Energy* **2019**, *237*, 210–226. [CrossRef]
36. Emadi, M.A.; Mahmoudimehr, J. Modeling and thermo-economic optimization of a new multi-generation system with geothermal heat source and LNG heat sink. *Energy Convers. Manag.* **2019**, *189*, 153–166. [CrossRef]
37. Wang, W.; Deng, S.; Zhao, D.; Zhao, L.; Lin, S.; Chen, M. Application of machine learning into organic Rankine cycle for prediction and optimization of thermal and exergy efficiency. *Energy Convers. Manag.* **2020**, *210*, 112700. [CrossRef]
38. Peng, Y.; Lin, X.; Liu, J.; Su, W.; Zhou, N. Machine learning prediction of ORC performance based on properties of working fluid. *Appl. Therm. Eng.* **2021**, *195*, 117184. [CrossRef]
39. Chen, W.; Liang, Y.; Luo, X.; Chen, J.; Yang, Z.; Chen, Y. Artificial neural network grey-box model for design and optimization of 50 MWe-scale combined supercritical CO2 Brayton cycle-ORC coal-fired power plant. *Energy Convers. Manag.* **2021**, *249*, 114821. [CrossRef]
40. Rumelhart, D.E.; McClelland, J.L. *Parallel Distributed Processing*; IEEE: Piscataway, NJ, USA, 1998.